The quasi-stationary feature of nocturnal precipitation in the Sichuan Basin and the role of the Tibetan Plateau

Xia Jin · Tongwen Wu · Laurent Li

Abstract The nocturnal precipitation in the Sichuan Basin in summer has been studied in many previous works. This paper expands the study on the diurnal cycle of precipitation in the Sichuan Basin to the whole year. Results show that the nocturnal precipitation has a specific quasi-stationary feature in the basin. It occurs not only in summer but also in other three seasons, even more remarkable in spring and autumn than in summer. There is a prominent eastward timing delay in the nocturnal precipitation, that is, the diurnal peak of precipitation occurs at early-night in the western basin whereas at late-night in the center and east of the basin. The Tibetan Plateau plays an essential role in the formation of this quasi-stationary nocturnal precipitation. The early-night peak of precipitation in the western basin is largely due to strong ascending over the plateau and its eastern lee side. In the central and eastern basin, three coexisting factors contribute to the late-night peak of precipitation. One is the lower-tropospheric southwesterly flow around the southeastern edge of the Tibetan Plateau, which creates a strong cyclonic rotation and ascendance in the basin at late-night, as well as brings abundant water vapor. The second is the descending motion downslope along the eastern lee side of the plateau, together with an air mass accumulation caused by the warmer air mass transport from the southeast of the Yunnan-Guizhou Plateau, creating a diabatic warming at low level of the troposphere in the central basin. The third is a cold advection from the plateau to the basin at late-night, which leads to a cooling in the middle troposphere over the central basin. All these factors are responsible for precipitation to occur at late-night in the central to eastern basin.

1 Introduction

The diurnal variation of precipitation is a significant aspect of weather and climate. It is often related to physical processes of local geography or regional atmospheric dynamics (e.g. Liu and Moncrieff (1998) and Lin et al. (2000) for a review on this topic). It is well known that the complex geographical environment in the Asian monsoon region can exert strong influences on the regional climate. Numerous studies have shown that there are remarkable diurnal characteristics of the precipitation in summer in the Asian monsoon region. Such studies use either rain-gauge measurements (e.g. Fujinami et al. 2005; Zhao et al. 2005; Yu et al. 2007a, b; Li et al. 2008) or satellite data (Zhou et al. 2008; Chen et al. 2009; Yu et al. 2009; He and Zhang 2010). The nocturnal precipitation in the Sichuan Basin in summer, i.e. the precipitation reaches its diurnal peak around midnight, becomes a hot topic in the recent decade (Li et al. 2008; Yu et al. 2007a, 2009; Chen et al. 2010; Huang et al. 2010; Bao et al. 2011; Yuan et al. 2011). This phenomenon has been observed and documented since long time (Lu 1942; Ye and Gao 1979; Zeng et al. 1994). But

X. Jin
Chinese Academy of Meteorological Sciences, China
Meteorological Administration, Beijing, China

X. Jin · L. Li
Laboratoire de Météorologie Dynamique, IPSL, CNRS/UPMC,
Paris, France

X. Jin · T. Wu (✉) · L. Li
National Climate Center, China Meteorological Administration,
46 Zhongguancun Nandajie, Beijing 100081,
People's Republic of China
e-mail: twwu@cma.gov.cn

only a few recent works have addressed the physical mechanisms in controlling the diurnal precipitation variation in summer in the Sichuan Basin (e.g. Dai et al. 2007; Yu et al. 2007a). Yu et al. (2007b) and Li et al. (2008) showed that the summertime nocturnal precipitation in the Sichuan Basin is contributed mainly by long-duration precipitating systems. In addition, the diurnal cycle of precipitation presents an eastward delayed diurnal phase from the east of the Tibetan Plateau (TP) down to the Yangtze River valley in central China (Chen et al. 2010; Huang et al. 2010; Bao et al. 2011; Yuan et al. 2011).

Several works proposed their assumptions to explain the summertime nocturnal precipitation in the Sichuan Basin. Li et al. (2003, 2008) suggested that it may be caused by a weakening of the mid-level inversion layer at night in summer. A numerical modeling study by Huang et al. (2010) on an individual event revealed that the eastern TP acts as a heat source for convection and a thermal driven diurnal solenoid circulation results in an ascendance over the Sichuan Basin in nighttime, which favors the nocturnal precipitation. And the diurnal variation of the solenoid circulation may contribute to the longevity and propagation of episodes in the vicinity of the eastern TP. Bao et al. (2011) employed the theory of mountain-plain solenoid propagation (may refer to Tripoli and Cotton 1989; Carbone and Tuttle 2008) to understand the phenomena of eastward delayed phase for precipitation in the Sichuan Basin. Chen et al. (2010) and Yuan et al. (2011) suggested that the summertime nocturnal precipitation was attributed to the decreasing stability caused by the low-tropospheric convergence and upward motion, accompanied by a long wave radiative cooling at the cloud top and the weak cold advection from the TP. These works have shown that the diurnal cycle of precipitation in summer is intimately linked to the topography in southwestern China.

Most previous studies on the diurnal variation of precipitation have focused on summer (June to August), the main rainy period in central China. However, the precipitation in the other seasons also accounts for a significant portion around the year. The regional average precipitation rates in the Sichuan Basin in spring (March to May) and autumn (September to November) account about 23 % of the total annual precipitation. In winter (December to February), the precipitation frequency is over 11 % (not shown). The purpose of this work is to explore the feature of diurnal cycle of precipitation in the Sichuan Basin in all the seasons and discuss the physical mechanisms involved in the diurnal cycle of precipitation.

The rest of the paper is organized as follows: Sect. 2 describes the dataset used in this work. Section 3 presents the characteristics of the diurnal precipitation cycle in the Sichuan Basin in different seasons. Section 4 analyzes the dynamic and thermodynamic effects of the TP on the diurnal cycle of precipitation in the Sichuan Basin. Conclusions are summarized in Sect. 5.

2 Data

The hourly $0.1° × 0.1°$ resolution merged precipitation products cover whole China from January 2008 to December 2010 (Yu et al. 2011; Shen et al. 2012). This dataset, produced by the National Meteorological Information Center of China Meteorological Administration, is used to study the diurnal cycle of precipitation. It combines the National Oceanic and Atmospheric Administration (NOAA)/Climate Prediction Center morphing technique (CMORPH) precipitation data (Joyce et al. 2004) and the hourly precipitation dataset observed by more than thirty thousand automatic meteorological stations in China (Fig. 1) (Shen et al. 2010a). As a high spatial/temporal precipitation dataset, CMORPH has better performance than many other satellite products over China (Shen et al. 2010b). However, the CMORPH dataset has systematic errors over China, characterized by an underestimation of strong precipitation and an overestimation of weak precipitation (Yu et al. 2011). So the ground observation precipitation dataset is used to correct the CMORPH data. The procedure to produce the merged precipitation products has mainly three steps: Firstly, the irregularly-distributed and quality-controlled hourly precipitation data derived from automatic meteorological stations are interpolated spatially into $0.1° × 0.1°$ gridded data through an optimal interpolation based on the climatological background (Shen et al. 2010a). Secondly, the 30-min 8-km resolution CMORPH satellite precipitation data are interpolated into hourly interval and $0.1° × 0.1°$ grid. Finally, systematic errors of CMORPH with respect to the ground observed precipitation are estimated to correct the CMORPH satellite precipitation. The systematic error is defined as a difference between the precipitation amounts corresponding to the same cumulative probability density for both datasets at every $0.1°$ longitude/latitude grid (Yu et al. 2011). As shown in Fig. 1, there are abundant automatic meteorological stations distributed in the Sichuan Basin where the precipitation observations have been involved in the merged precipitation products. This dataset is believed to have a very good quality in the Sichuan Basin.

In order to characterize the atmospheric dynamical and thermo-dynamical states which are in close relationship with the diurnal behavior of precipitation, we use a subset of the ERA-Interim reanalysis data (Dee et al. 2011). This dataset has a $0.75° × 0.75°$ resolution and outputs at 6 h interval at 00, 06, 12 and 18 UTC. The period from January 2003 to December 2010 is used in this study.
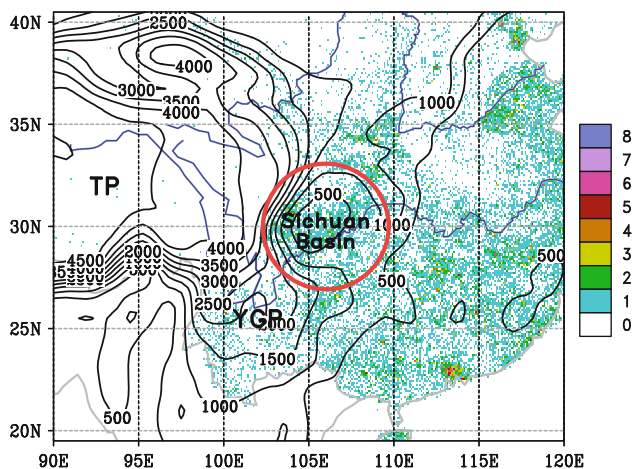
Fig. 1 Terrain distribution (unit: m; *contoured in black solid*) over the South of China and density distribution of the automatic meteorological stations (*colored*; different colors denote number of stations in each $0.1° \times 0.1°$ grid area). The Yangtze River and the Yellow River are plotted in *blue*. TP and YGP are short for the Tibetan Plateau and the Yunnan-Guizhou Plateau, respectively. The Sichuan Basin is marked with a *red circle*

3 Characteristics of diurnal cycle of precipitation

The diurnal peaks of seasonally-averaged hourly precipitation frequency and rate for four seasons over the south of China are shown in Figs. 2 and 3, respectively. The methodology used here is based on an explicit maximum selection. Hourly period in local solar time (LST) during which the precipitation frequency (or rate) reaches its maximum in 1 day at each $0.1° \times 0.1°$ grids are marked. Light colors stand for daytime peaks whereas dark colors are related to nighttime peaks.

As shown in Fig. 2, in the Sichuan Basin (encircled in a red circle), the maximal precipitation frequency occurs at nighttime (1800–0600LST) in all the seasons, which is remarkably different from an afternoon (1200–1800LST) frequency peak in most other areas of the continent. In spring (Fig. 2b), the area with nocturnal peaks of precipitation frequency is most pronounced among these four seasons. It covers the whole Sichuan Basin and a large area to the east of the Yunnan-Guizhou Plateau (YGP), which is
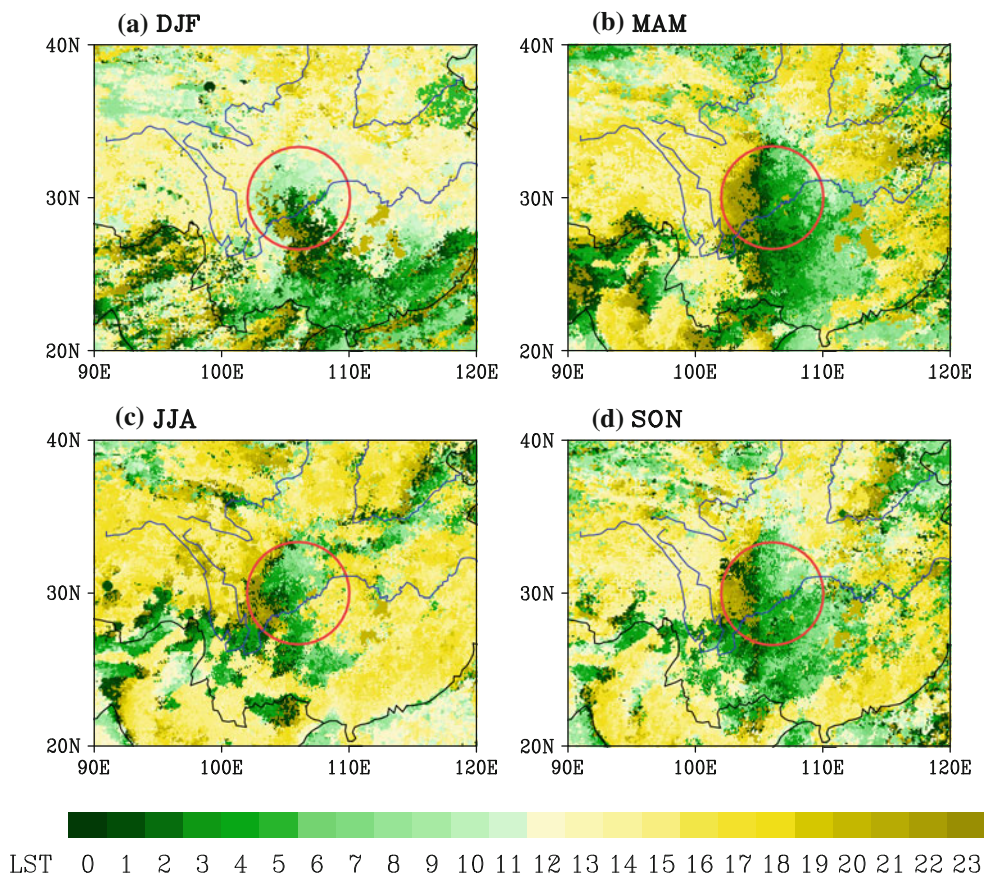

Fig. 2 Local solar time (LST) of diurnal peaks for precipitation frequency as derived from hourly merged precipitation products at each $0.1° \times 0.1°$ grid for the seasons of **a** December–January–February (DJF), **b** March–April–May (MAM), **c** June–July–August (JJA) and **d** September–October–November (SON) from 2008 to 2010. The Yangtze River and the Yellow River are plotted in *blue*. The Sichuan Basin is marked with a *red circle*
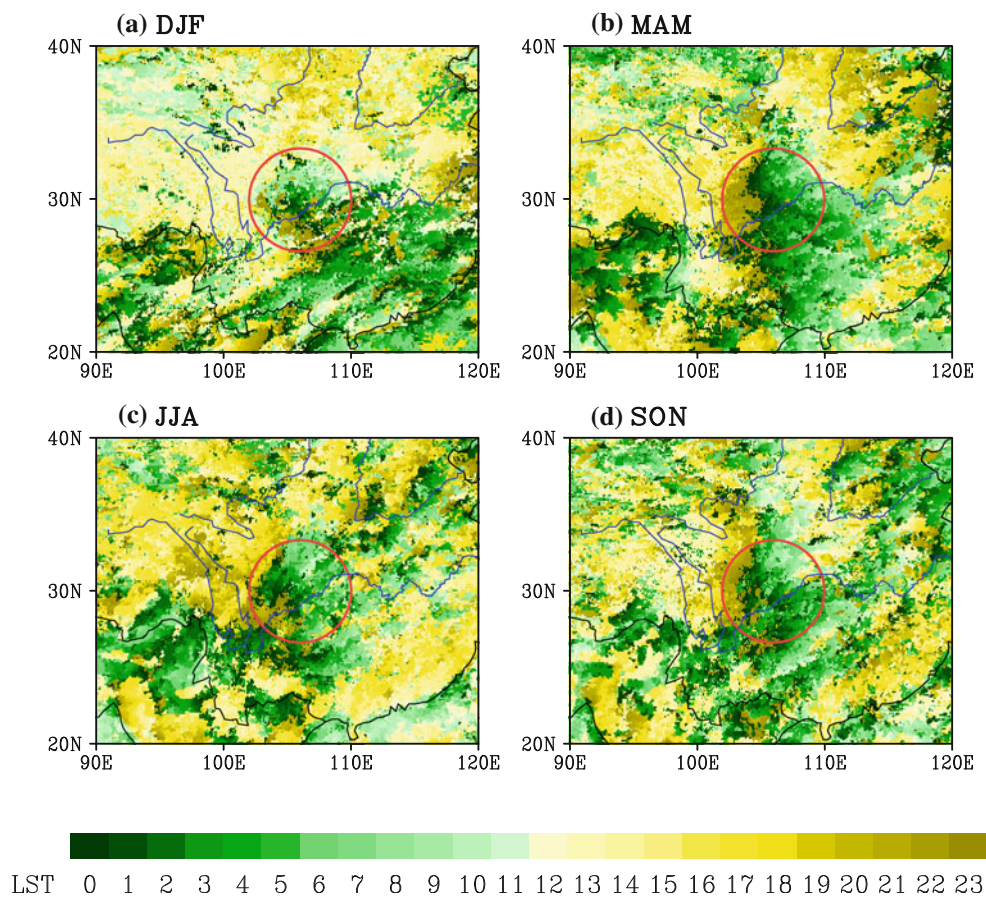
Fig. 3 Same as in Fig. 2 but for precipitation rate

located in the southwest of the Sichuan Basin (as shown in Fig. 1). It even spreads to the south of the YGP. In autumn (Fig. 2d), the area with the highest precipitation frequency at night is not as large as in spring but still significant. It covers most of the basin and the region to the eastern slope of the YGP. In winter (Fig. 2a), the nocturnal peaks of precipitation frequency still exist in the basin, but is mainly located in the south of the basin, the east of the YGP and the coastal region of South China. In summer (Fig. 2c), the area with the most frequent nocturnal precipitation is mainly located inside the basin, which is smaller than that in spring and autumn. We also note that in the eastern basin, the peak of diurnal cycle of precipitation frequency in summer has its specificity and appears in afternoon but not at nighttime. It is possibly caused by a stronger local mountain heating in the afternoon of summer season. No matter how the area varies by season, the maximal precipitation frequency in the Sichuan Basin generally appears at nighttime through the whole year.

It is noted that the color transition from brown to green in the Sichuan Basin exhibits an eastward phase delay for the maximal precipitation frequency in all seasons (Fig. 2), which is significant especially in spring and autumn.

In spring, the maximum precipitation frequency timing shows a highly regular transition from west to east in the basin. That is, the early-night (1800–0000LST) peaks appear in the western basin (west of 105°E) while the late-night peaks (0000–0600LST) always occur in the central to eastern basin (east of 105°E). This phenomenon can also be observed in autumn and summer. In winter, an eastward delay still exists, although the area with frequent nocturnal precipitation has moved to the south of the basin.

The geographic distribution of peak timing for seasonally-averaged hourly precipitation rate (Fig. 3) in the Sichuan Basin shows similar spatial features as for precipitation frequency (Fig. 2). The diurnal maximal precipitation occurs at nighttime in the basin and also presents a longitudinal phase-delay in most of the seasons. The discrepancy between west and east of the basin is obvious in spring, summer and autumn. The diurnal variation of precipitation rate peaks at early-night (1800–0000LST) over most of the western basin and at late-night (0000–0600LST) in the central and eastern basin, respectively. In winter, this phenomenon is not as conspicuous as in other three seasons whereas it can still be distinguished. In addition, some differences in summer are observed in

Fig. 4 Time-longitude diagrams of hourly precipitation (mm h^{-1}) averaged between 28°N and 32°N for **a** DJF, **b** MAM, **c** JJA and **d** SON. Vertical axis indicates time in UTC. *Diagonal lines* are lines of equal local solar time
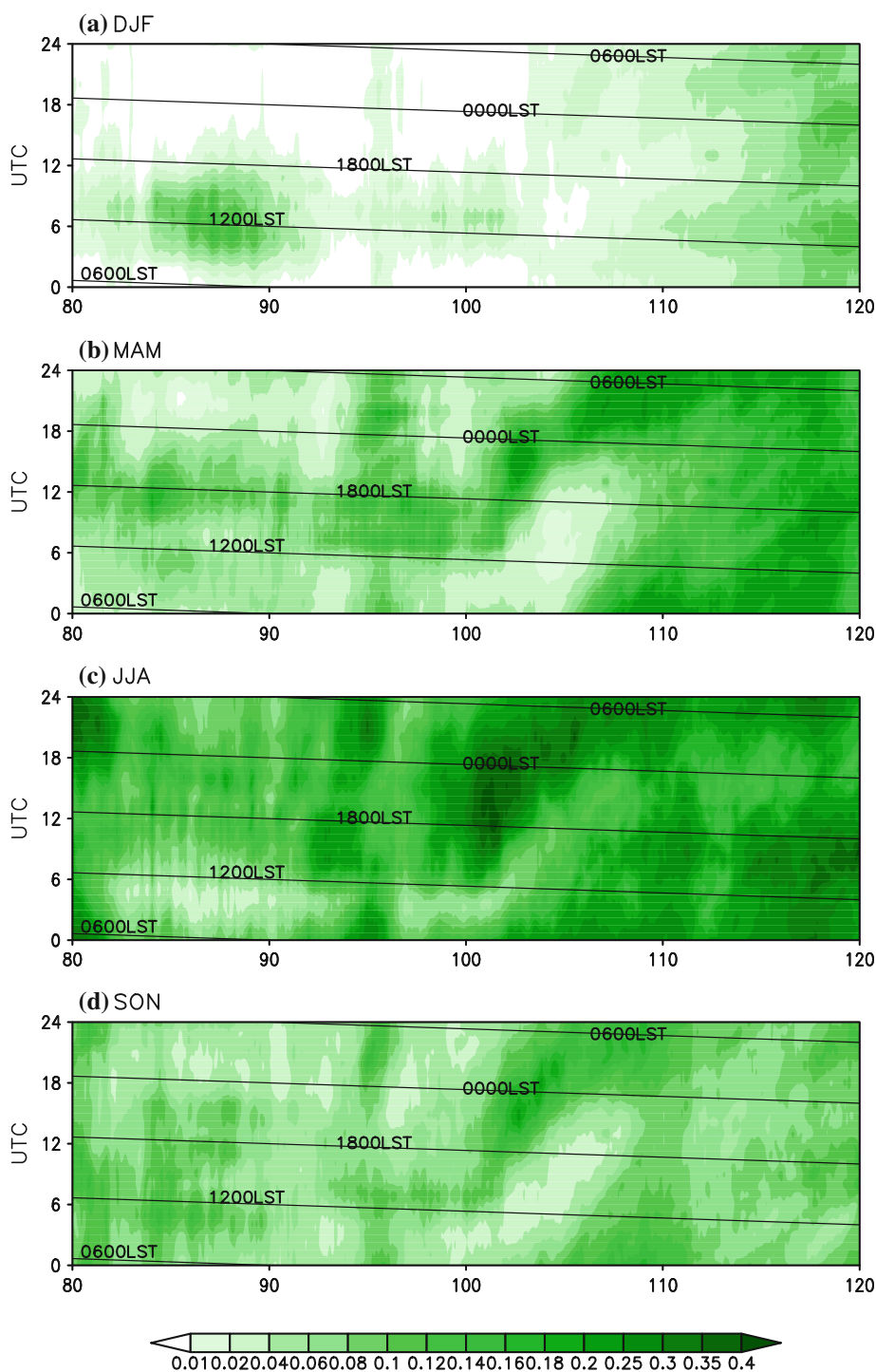

Fig. 3c with respect to Fig. 2c. In the southeastern part of the basin, the maximal precipitation rate appears in the morning (0600–1200LST), whereas the maximal precipitation frequency occurs in the afternoon (1200–1800LST).

Figure 4 shows the Hövmoller diagram of seasonally mean of hourly precipitation for the latitude band between 28°N and 32°N. There exists an obvious eastward timing delay for precipitation maximum from the east of the TP (about 93°E–100°E) to the eastern plain in four seasons. A propagation of precipitation seems to originate from the TP and moves eastward to the Sichuan Basin. However, when we view all individual precipitation events in the period from January 2008 to December 2010, it is found that most of them are originated from the basin (for example in Figs. 5a–c). Only few cases of precipitation begin from the TP and then propagate eastward to the basin in summer
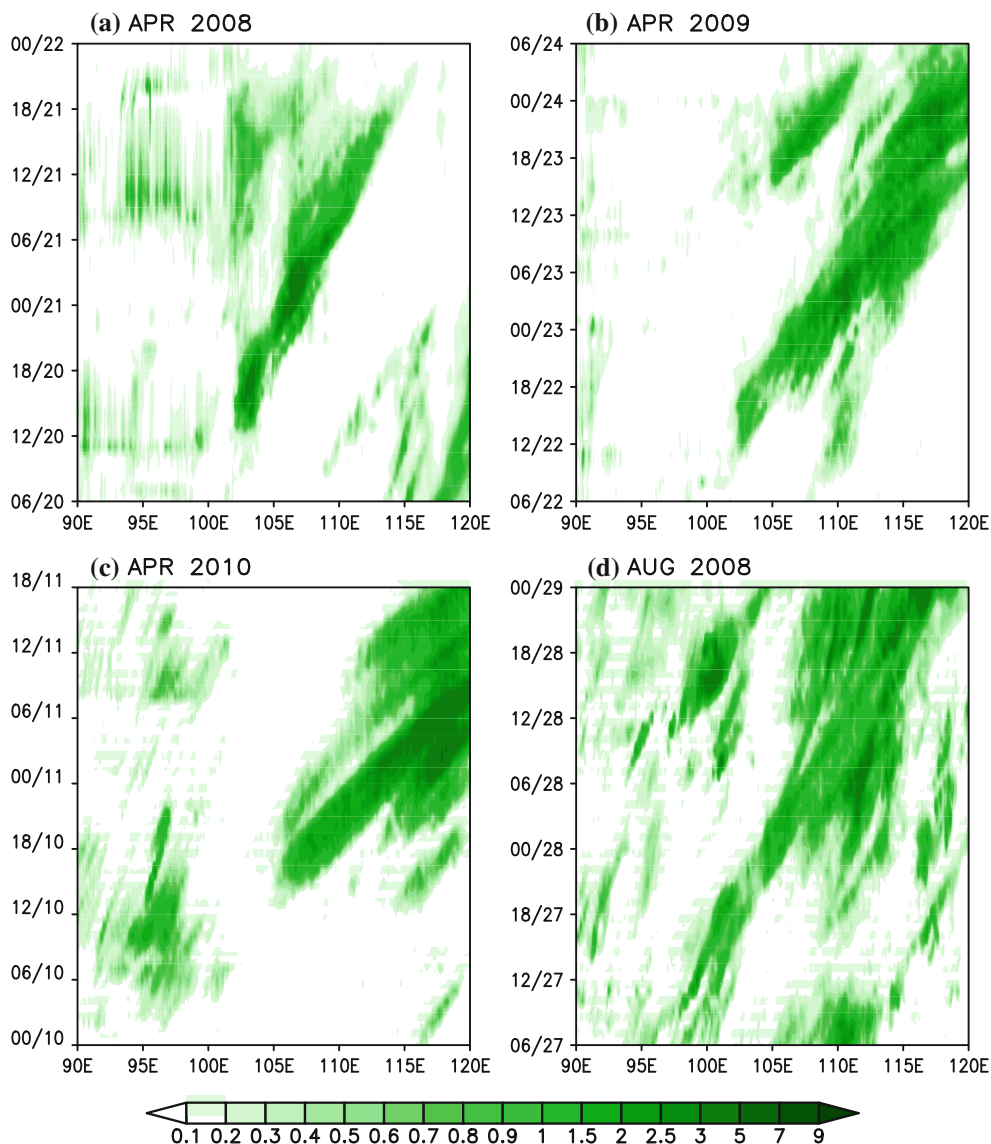
Fig. 5 Time-longitude diagrams of hourly precipitation (mm h^{-1}) averaged between 28°N and 32°N for **a** 0600UTC 20th—0000UTC 22th, April 2008, **b** 0600UTC 22th—0600UTC 24th, April 2009, **c** 0000UTC 10th—1800UTC 11th, April 2010 and **d** 0600UTC 27th—0000UTC 29th, August 2008

(for example in Fig. 5d). If we average these four cases of precipitation shown in Fig. 5, it would show a continuous precipitation process from the TP to the eastern basin which is similar to the pattern shown in Fig. 4.

4 Role of the TP in the quasi-stationary nocturnal precipitation

Although the summertime nocturnal precipitation in the Sichuan Basin has been explored in many previous studies, the above analyses further show that the nocturnal peak of diurnal precipitation cycle exists steadily in all seasons, and the nocturnal precipitation is even more significant in

spring and autumn than in summer. The quasi-stationary behavior of the nocturnal precipitation peak gives us the intuition that it must be strongly related to the topography of the region.

The Sichuan Basin is adjacent to the eastern side of the TP and the northeastern slope of the YGP. To its east, the basin is surrounded by a series of small mountains with an average altitude of 1,000 m (Fig. 1). The TP and the YGP are the most significant highlands over the southwest of China. The main body of the TP has an average elevation of over 4,000 m above sea level (near 600 hPa). The YGP, which is located in Yunnan and Guizhou provinces in Southwestern China and adjacent to the southeast of the TP, is over 2,000 m in elevation. The area of YGP is much
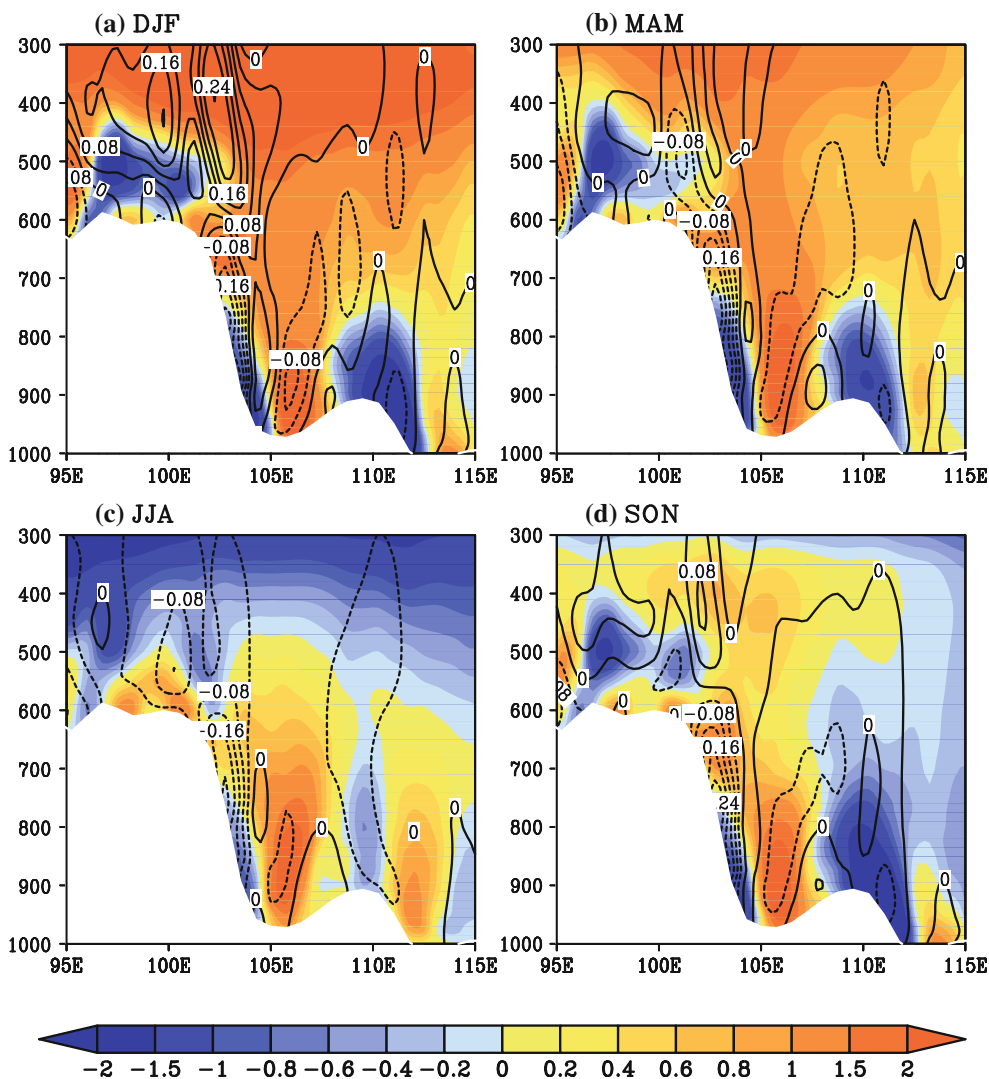
Fig. 6 Profile of seasonal mean relative vorticity (10^{-5} s^{-1}, *shaded*) and vertical velocity (Pa s^{-1}, *contour*) along the latitude of 30°N for **a** DJF, **b** MAM, **c** JJA and **d** SON. The interval of contours is 0.04 Pa s^{-1}. Topography is *shaded* in *white*

smaller than that of the TP, and the altitude of the YGP decreases gradually from northwest to southeast, which looks like a stretch of the southeast of the TP, so hereafter we put the YGP together with the TP as a united plateau for the convenience of discussion. In this section, two main aspects are analyzed: dynamical forcing and thermal dynamical effect of the plateau. In this section, the LST is according to the center of the Sichuan Basin (30°N, 105°E).

4.1 Influences of large-scale dynamical forcing of the plateau

Figure 6 depicts the profile of climatological mean relative vorticity and vertical velocity along the latitude of 30°N. On the impact of the TP terrain, the lower troposphere in the southeast periphery of the TP is dominated by the southwesterly wind in DJF, MAM and JJA and the southeasterly wind in SON. A steady deep cyclonic vorticity forms over the eastern slope of the TP. The strong positive vorticity dominates the low level of the troposphere (from surface to 750 hPa) in the central and eastern basin (from 105°E to 108°E). It stretches upward to the middle level of the troposphere (approximately 500 hPa). This quasi-stationary positive vorticity in the center and east of the Sichuan Basin is well correspondent to the upward motion which favors atmospheric instabilities and a center of precipitation in the Sichuan Basin (not shown) in all seasons.

The cyclonic vorticity in the basin has a conspicuous diurnal variation. Figure 7 describes the diurnal cycle of relative vorticity and wind at 800 hPa level in different seasons. The positive relative vorticity in the central basin is apparently stronger at nighttime than at daytime in all seasons, which is in accord with the local ascendance and
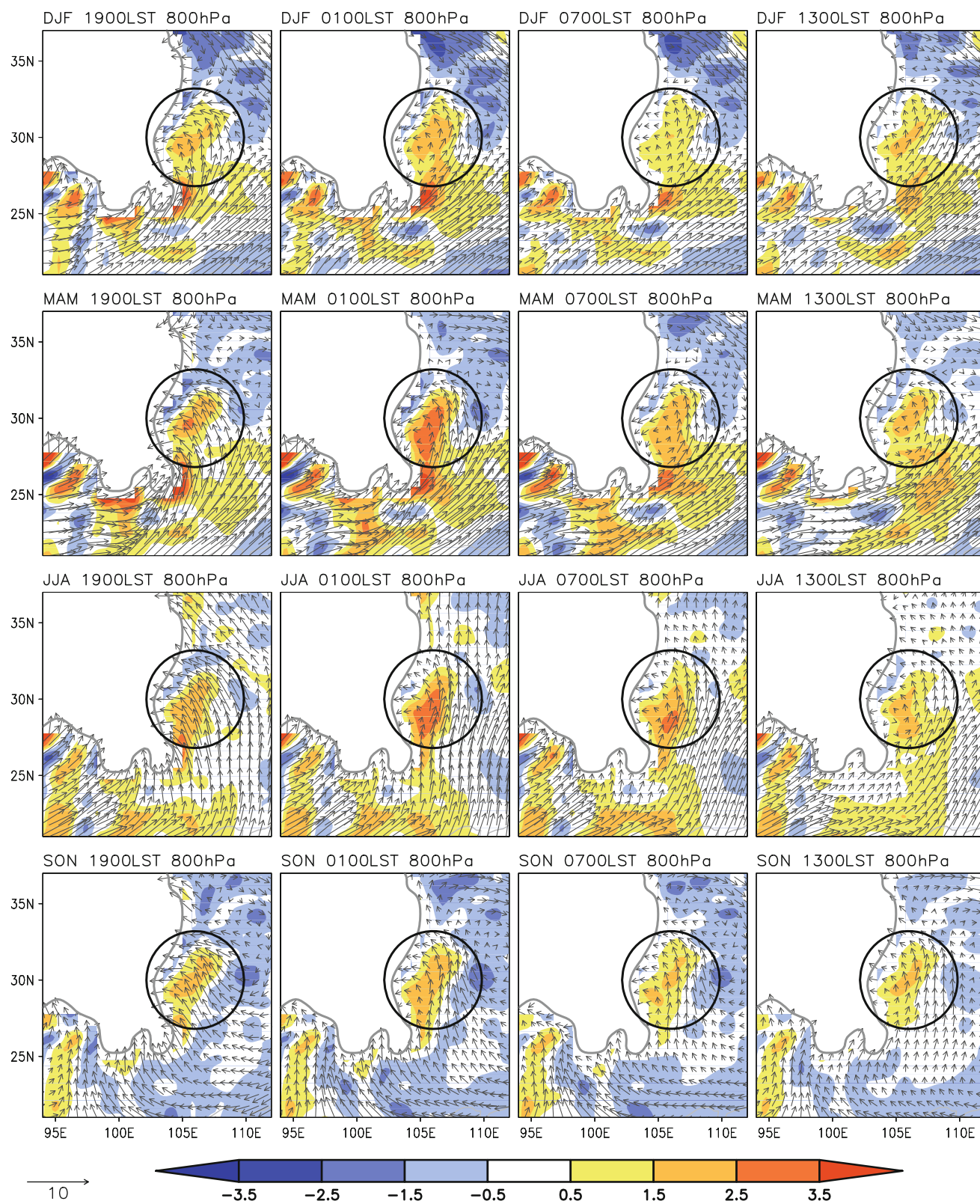
Fig. 7 Diurnal cycle of relative vorticity (10^{-5} s^{-1}, *shaded*) and wind (m s^{-1}, *vector*) at 800 hPa for the seasons of (*top row*) DJF, (*second row*) MAM, (*third row*) JJA and (*bottom row*) SON. From *left to right*, the columns are for 1900LST, 0100LST, 0700LST and 1300LST, respectively. The 2,000 m height contour is sketched with *grey thick line*. The Sichuan Basin is marked with a *black circle*
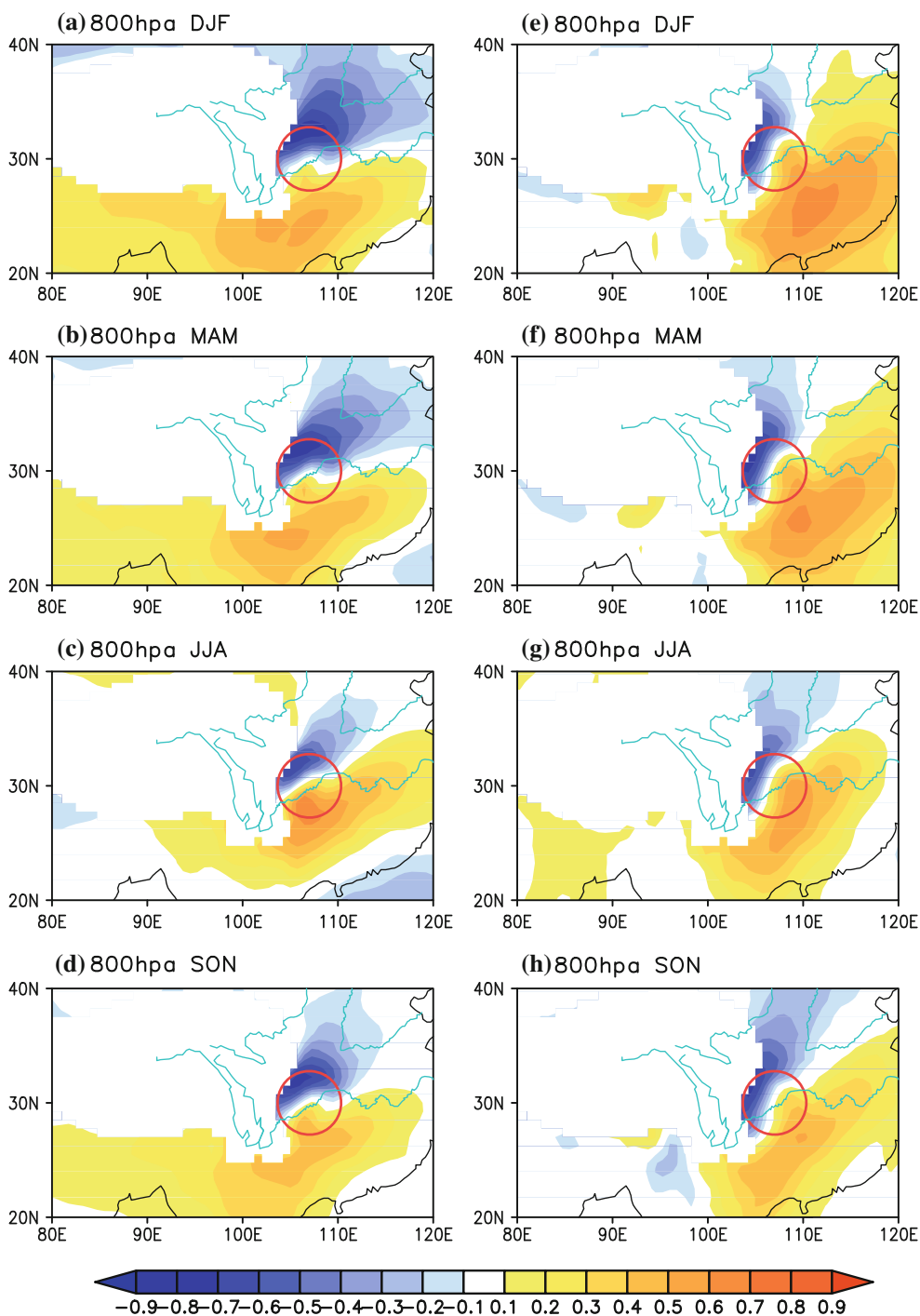
Fig. 8 Correlation between regional averaged relative vorticity in the Sichuan Basin and (*left column*) zonal wind field and (*right column*) meridional wind field over 800 hPa at 0100LST for **a**, **e** DJF, **b**, **f** MAM, **c**, **g** JJA and **d**, **h** SON. The correlation coefficient over 0.2 is significant at the 99.9 % confidence level as determined by the Student's *t* test. The Sichuan Basin is marked with a *red circle*

precipitation at late-night. The strongest positive relative vorticity almost occurs at 0100LST, while the weakest one appears at 1300LST. In spring and summer, the strength of this positive relative vorticity varies most significantly, as the diurnal variation range achieves $2 \times 10^{-5} \text{ s}^{-1}$.

The diurnal variation of the relative vorticity in the central basin is intimately associated with that of the wind. As shown in Fig. 7, the southwesterly wind in spring, summer and winter prevails in southeast of the TP. It flows around the southeastern periphery of the YGP and enters
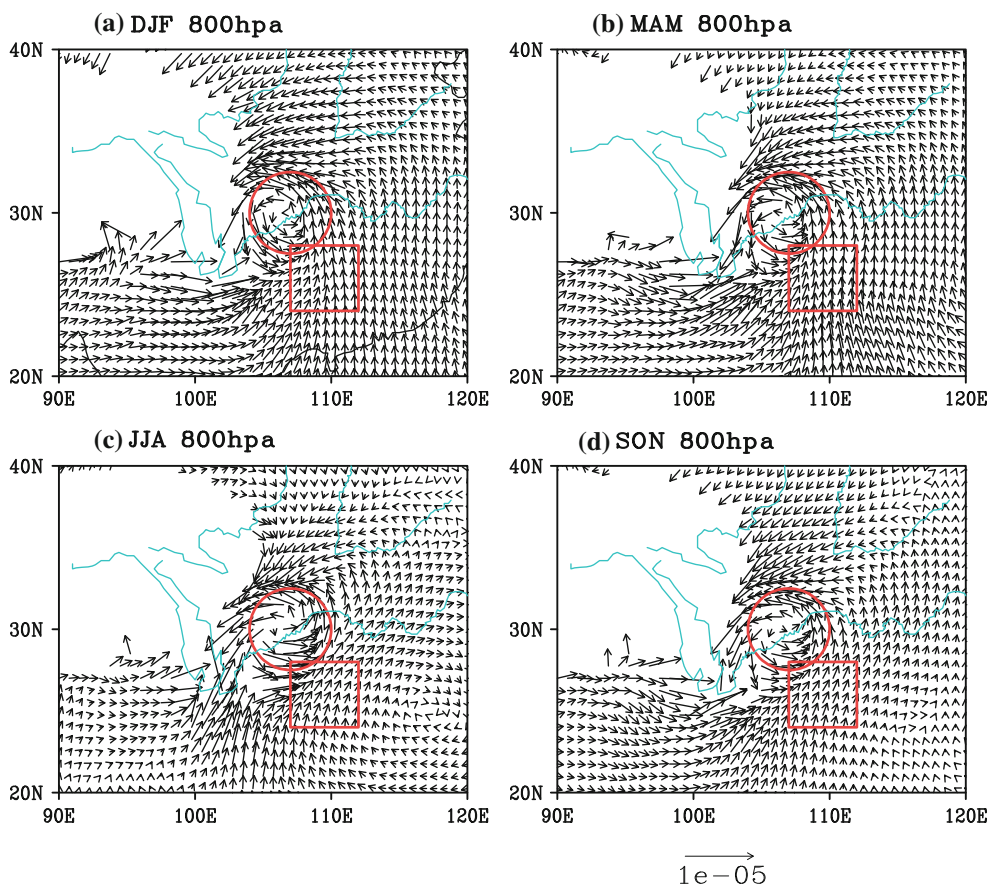
(a) DJF 800hpa

(b) MAM 800hpa

(c) JJA 800hpa

(d) SON 800hpa

$\overrightarrow{1e-05}$

Fig. 9 The spatial distribution of vectors ($A_{(i, j)}$, $B_{(i, j)}$), whose components are the coefficients of dualistic linear regression ($vort_{basin} = A_{(i,j)} \times u_{(i,j)} + B_{(i,j)} \times v_{(i,j)} + C_{(i,j)}$) of the regional averaged relative vorticity in the Sichuan Basin ($vort_{basin}$) on the horizontal wind ($u_{(i, j)}$, $v_{(i, j)}$) at each grid over 800 hPa for 0100LST for **a** DJF, **b** MAM, **c** JJA and **d** SON. The unit is m^{-1}. The Sichuan Basin is marked with a *red circle*. The area (24°N–28°N, 107°E–112°E) is marked with a *red rectangle*

the eastern part of the basin through the lower mountain in the southeast of the basin. Due to the topographic forcing of the concave basin, this flow causes a strong cyclonic rotation in the central basin. In autumn, although southeasterly flow dominates a large area over the southeast of the TP, by the obstruction of the YGP, it turns its direction to north and flows around the eastern periphery of the YGP and goes into the basin, and finally forms a cyclonic rotation similar to that in other three seasons in the central basin.

Figure 8 gives a clear association between the regional average relative vorticity in the basin and gridded zonal/meridional wind velocity over East Asia at 800 hPa for 0100LST. The spatial correlations shown in Figs. 8a–d presents that the relative vorticity in the Sichuan Basin is positively correlated to the westerly wind over a large area in the southeast periphery of the YGP. Especially in spring (Fig. 8b) and winter (Fig. 8a), the region of high positive correlation coefficients is located in the south and southeast slope of the YGP where the westerly wind prevails. As a result of the cyclonic rotation in the basin, positive

correlation is found in south of the basin and negative correlation in north of the basin in the four seasons. In Fig. 8e–h, a large area of positive correlation between relative vorticity in the basin and the gridded meridional wind velocity is located in the southeast slope of the YGP in all the seasons, which denotes that the strengthening of the southerly wind in this region has a strong relationship with the increasing positive relative vorticity in the central basin at late-night.

Figure 9 shows the spatial distribution of vectors ($A_{(i, j)}$, $B_{(i, j)}$), whose components are the coefficients of dualistic linear regression ($vort_{basin} = A_{(i,j)} \times u_{(i,j)} + B_{(i,j)} \times v_{(i,j)} + C_{(i,j)}$) of the regional averaged relative vorticity in the Sichuan Basin ($vort_{basin}$) on the horizontal wind ($u_{(i, j)}$, $v_{(i, j)}$) at each grid over 800 hPa for 0100LST. The direction of vector at each grid denotes the wind direction exerting influence on the relative vorticity in the basin, and the length of the vector quantifies the intensity. It shows high consistency in all of the seasons. Long vectors are on the slope of the mountain around the basin and in the southeastern periphery of the YGP. Vectors surrounding the
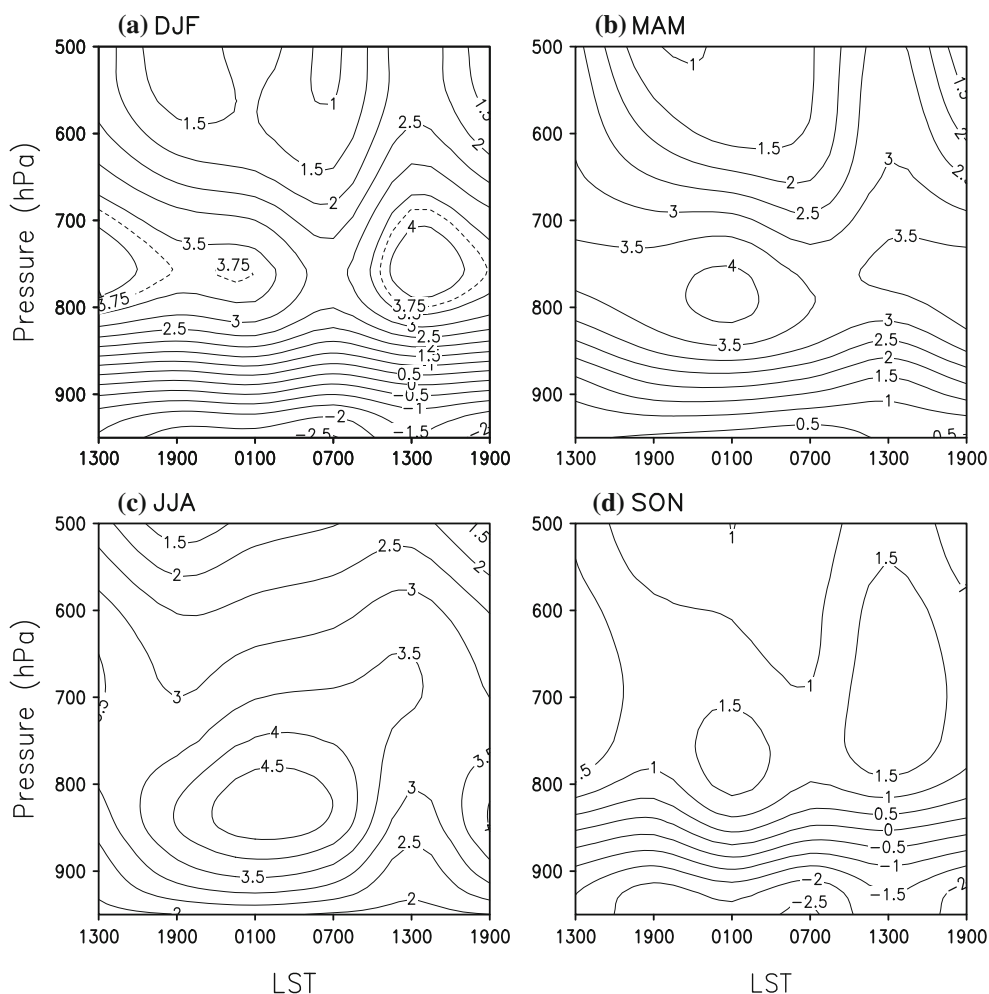
Fig. 10 Diurnal cycle of regionally-averaged meridional wind (m s^{-1}) in the area (24°N–28°N, 107°E–112°E) as marked in Fig. 9 for the seasons of **a** DJF, **b** MAM, **c** JJA and **d** SON. The horizontal axis signifies the LST and the vertical axis denotes the barometric height (hPa)

basin turn cyclonically due to orographic forcing. The southerly and southwesterly winds dominate the region in the southeastern side of the YGP and play an important role on the variation of relative vorticity in the central basin at late-night in four seasons.

As illustrated in Figs. 8 and 9, it implies that the diurnal variation of the southwesterly wind around the southeast vicinity of YGP has an essential role on the diurnal cycle of the low-tropospheric relative vorticity in the basin. Figure 10 presents the diurnal cycle of averaged meridional wind over the southeast periphery of YGP (24°N–28°N, 107°E–112°E). It shows a positive center of southerly wind at low level of the troposphere (from 850 hPa to 750 hPa) at 0100LST in different seasons, which exactly corresponds to the strongest positive relative vorticity in the basin (Fig. 7).

In addition, the low-tropospheric southwesterly wind also brings more moisture at night, which favors the nocturnal precipitation. Figure 11 shows the climatological

background of meridional water vapor transport in the atmospheric column from surface to 500 hPa for four seasons. Accompanying the low-level southwesterly, moisture from the south enters the eastern basin through its opening in the southeast in all seasons. It has an effect to the precipitation in the central and eastern basin. Note that there is less water vapor transport directly from the south in the western part of the Sichuan Basin because of the terrain obstruction. It seems that the air flow coming from the southeast periphery of the TP can not directly affect the rainfall in the western part of the basin.

Significant differences between west and east of the basin also exist in the diurnal variation of the atmospheric water vapor content integrated from surface to 500 hPa. As shown in Fig. 12, the maximal water vapor content in the western basin (102°E–104°E) appears at early-night (1800–0000LST) in all the seasons, which is beneficial for early-night precipitation. However, in the central and eastern basin (105°E–108°E), the maximal water vapor content
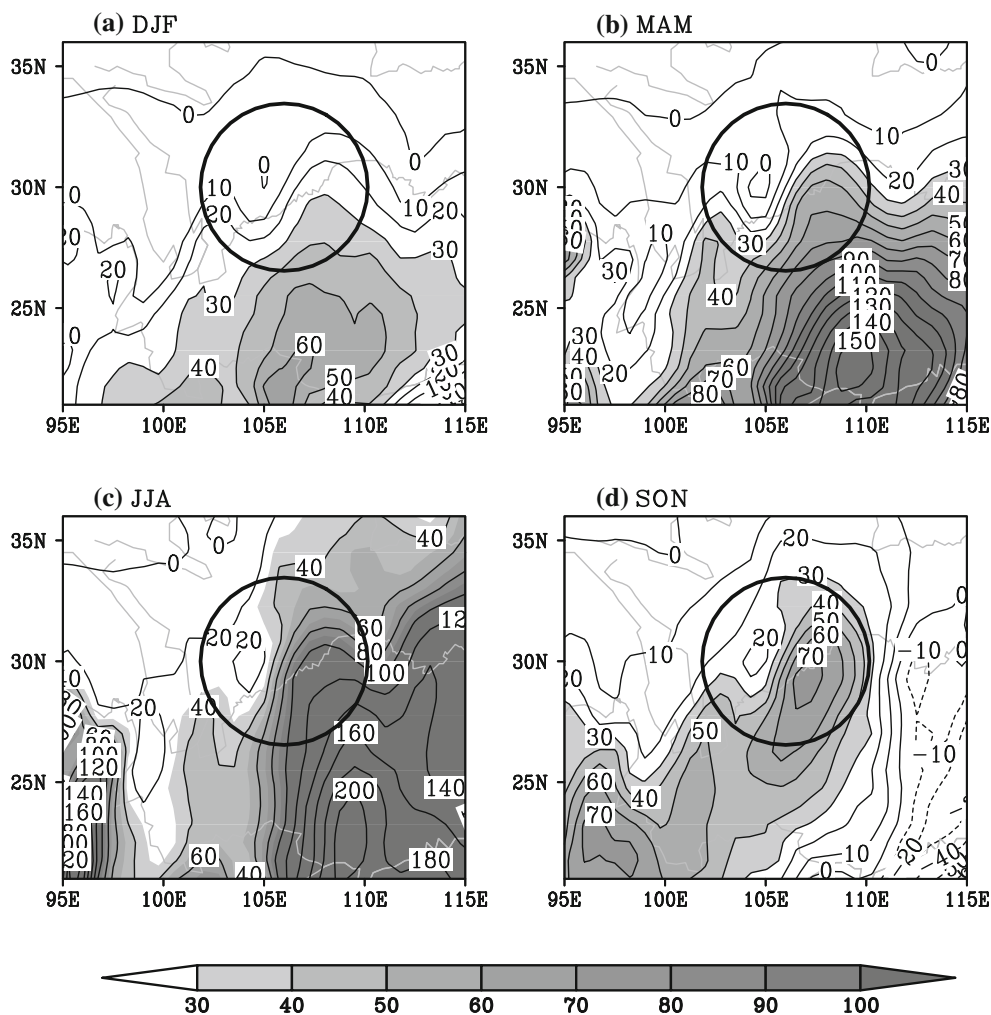
Fig. 11 Seasonally-mean and vertically-integrated meridional water vapor transport from surface to 500 hPa ($\int_{surf}^{500} qvdp$, unit: 10^2 kg s^{-3}) for **a** DJF, **b** MAM, **c** JJA and **d** SON. The Sichuan Basin is marked with a *black circle*

occurs at late-night (0000–0600LST), favorable for precipitation after midnight.

### 4.2 Thermal dynamical effect of the TP

The Sichuan Basin is located in the downstream of the westerly wind from the TP. The atmospheric circulation over the TP has an important influence on the diurnal variation of precipitation in the Sichuan Basin, which is closely related to the atmospheric temperature variation over the TP.

The diurnal variation of potential temperature over 550 hPa, which is close to the surface of the TP, is shown in Fig. 13. Although potential temperature experiences considerable seasonal variation, it still varies regularly at diurnal scale. It is evident that the strongest diurnal anomalous potential temperature (both positive and negative values) occurs over the TP. The potential temperature near the surface of the TP at daytime is obviously warmer

than that during nighttime. The warmest near-surface temperature occurs at 1900LST and the coldest at 0700LST. After sunset (near 1900LST), the near-surface potential temperature drops dramatically and continues to decrease during the whole night until the sunrise (near 0700LST). The diurnal variation of atmospheric potential temperature over the TP ranges between +2 and −2 K in contrast to the daily mean. However, the potential temperature at 550 hPa in the basin varies much more moderately, as the variation range is only between +0.5 and −0.5 K.

Such a significant diurnal variation of potential temperature over the TP has a great influence on the atmospheric circulation. As presented in Fig. 13, at daytime, the warming over the TP causes arising motion and convergence near the surface of the TP. The strongest convergence appears at 1900LST. During nighttime, the continuous cooling over the TP leads to subsidence and

Fig. 12 Time-longitude diagrams of the anomaly from daily mean of integrated specific humidity from surface to 500 hPa ($\int_{surf}^{500} qdp$, unit: 10^2 kg m^{-1} s^{-2}) averaged from 28°N to 32°N for **a** DJF, **b** MAM, **c** JJA and **d** SON. The vertical axis signifies the LST
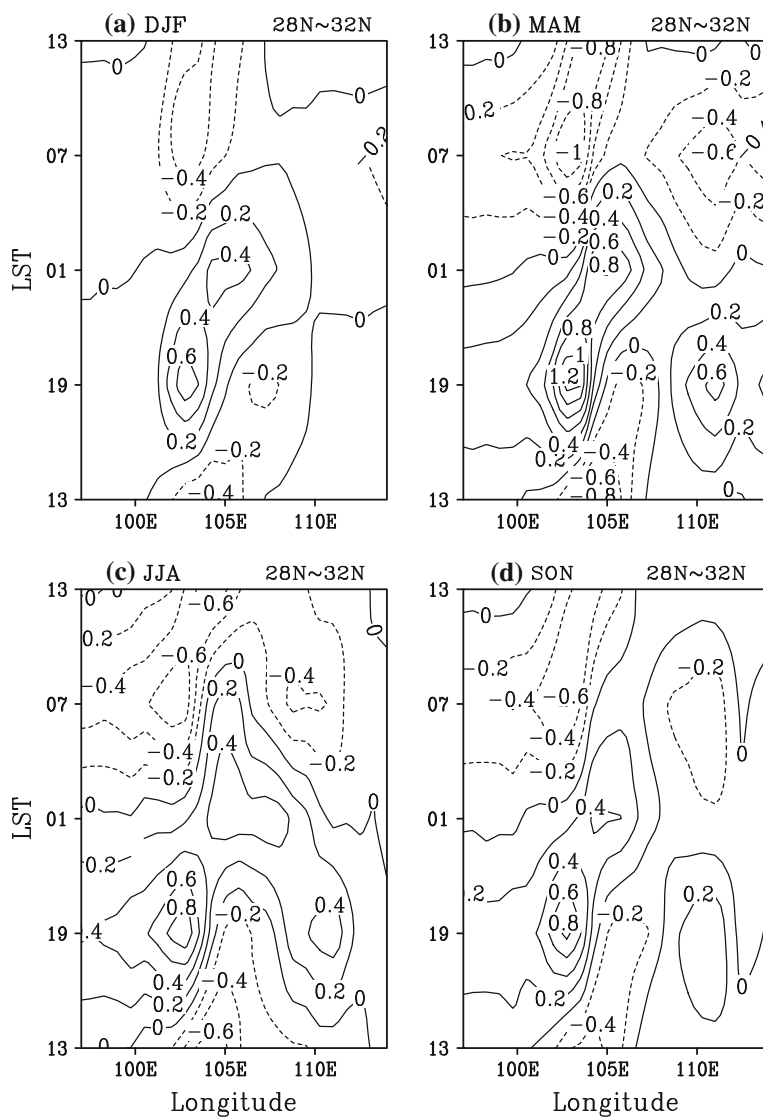
divergence over the near-surface of the TP. As the surface of the TP is colder and colder, the strengths of the subsidence and the divergence are increasing during the whole night and reach their strongest values at 0700LST.

Figure 14 presents the vertical profile of diurnal cycle of anomaly from daily mean of the potential temperature and circulation in the cross section along 30°N. It is clear that at 1900LST, the ascendance caused by strong warming over the TP dominates the TP and its eastern vicinity. The western basin is controlled by upslope wind at early-night, which is favorable for precipitation. At the same time, there is a compensating descending motion suppressing precipitation in the center and east of the basin, as the lower-troposphere water vapor source in the western basin mainly comes from the central to eastern basin and less water transporting directly from the south (Fig. 11). They construct a solenoidal circulation at the lower to middle level in the basin. At 0100LST, as the temperature drops over the

near-surface of the TP, descending motion controls the TP. The downdraft flow downslope along the eastern lee side of the plateau to the central basin. There is a relatively warmer center in the central basin at lower level of the troposphere (from 900 to 800 hPa). It is possibly caused by the diabatic descent warming and accumulation of warmer air mass coming from the southeastern edge of the YGP in the basin. This anomalous warm air mass is easily to cause the middle troposphere (about 800 hPa) getting more instability at late-night than other times. The relatively warm air arises in the central and eastern basin and the downslope flow in the western basin construct an anomalous solenoidal circulation at the lower- to mid-troposphere in the basin.

As shown in Fig. 14, along with the development of cooling over the TP at late-night, the anomalous downward motion near the surface of the TP is more and more intensified and even spreads to the mid-troposphere in the
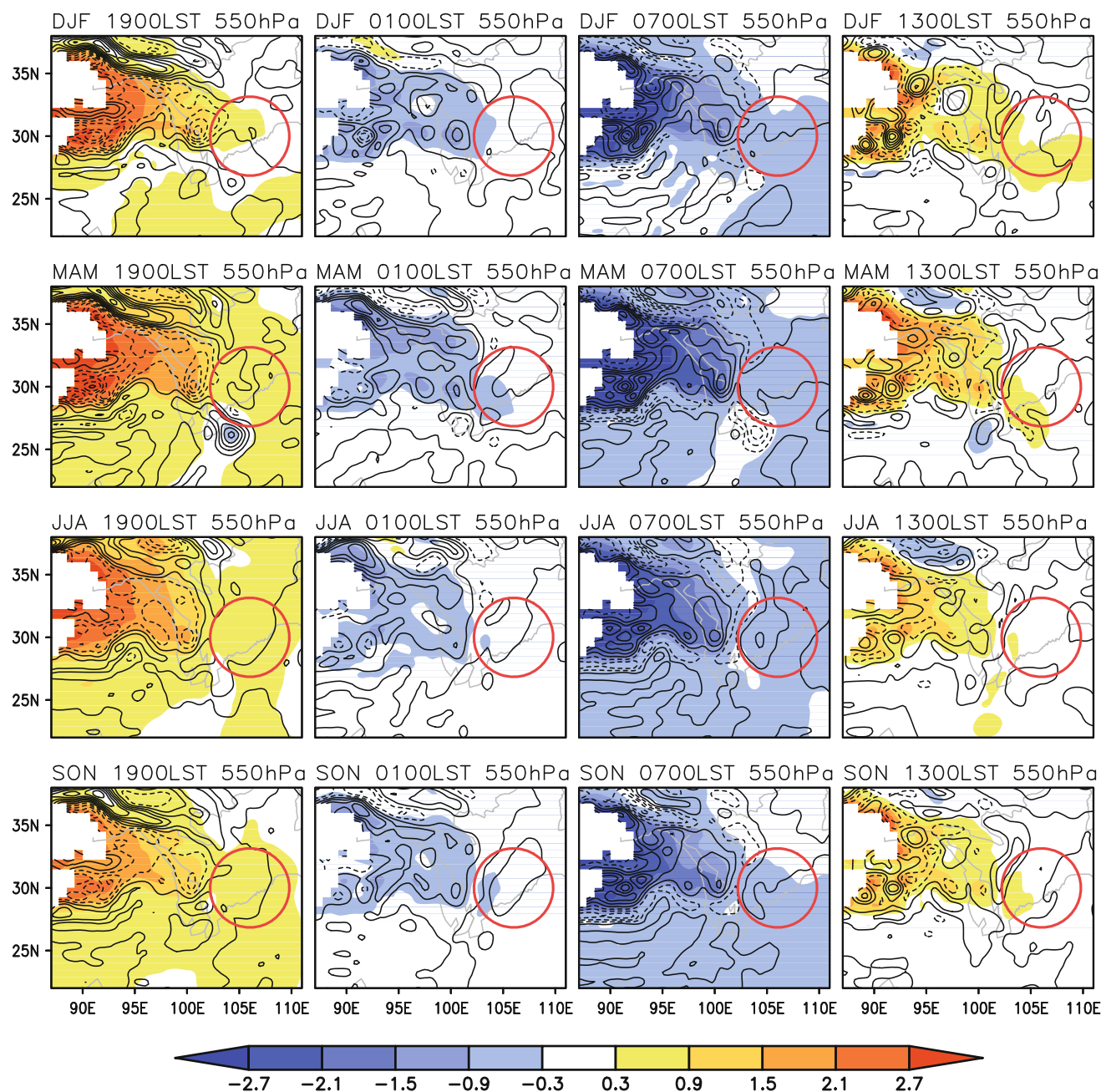
Fig. 13 Anomalous (by the daily mean) diurnal cycle of potential temperature (K, *shaded*) and divergence (10^{-6} s^{-1}, *contour*) at 550 hPa for (*top row*) DJF, (*second row*) MAM, (*third row*) JJA and (*bottom row*) SON. From *left* to *right*, the columns are for 1900LST, 0100LST, 0700LST and 1300LST, respectively. The contour intervals are 5×10^{-6} s^{-1}. The Sichuan Basin is marked with a *black circle*

basin. In addition, the hill in the east of the basin also gets cooling before sunrise. The anomalous ascending motion at late-night in the low hill in the east of the basin is gradually changed to anomalous descending motion before sunrise. After sunrise, the anomalous descending motion in the east of the basin is gradually replaced by ascending motion.

As the altitude of the TP is above 600 hPa, the strong cooling and divergence near the surface of the TP at night cause an eastward cold advection from the plateau and

leads to a cooling at the middle troposphere in the basin. Figure 15 shows the diurnal cycle of zonal advection of potential temperature at 550 hPa at the location of the central basin (30°N, 105°E). In winter, spring and autumn, there is a cold advection after midnight. In summer, the cold advection is not as strong as in other seasons. But the warm advection is very weak (almost zero) at late-night. This eastward cold advection at middle level of the troposphere encounters the warmer updraft with abundant
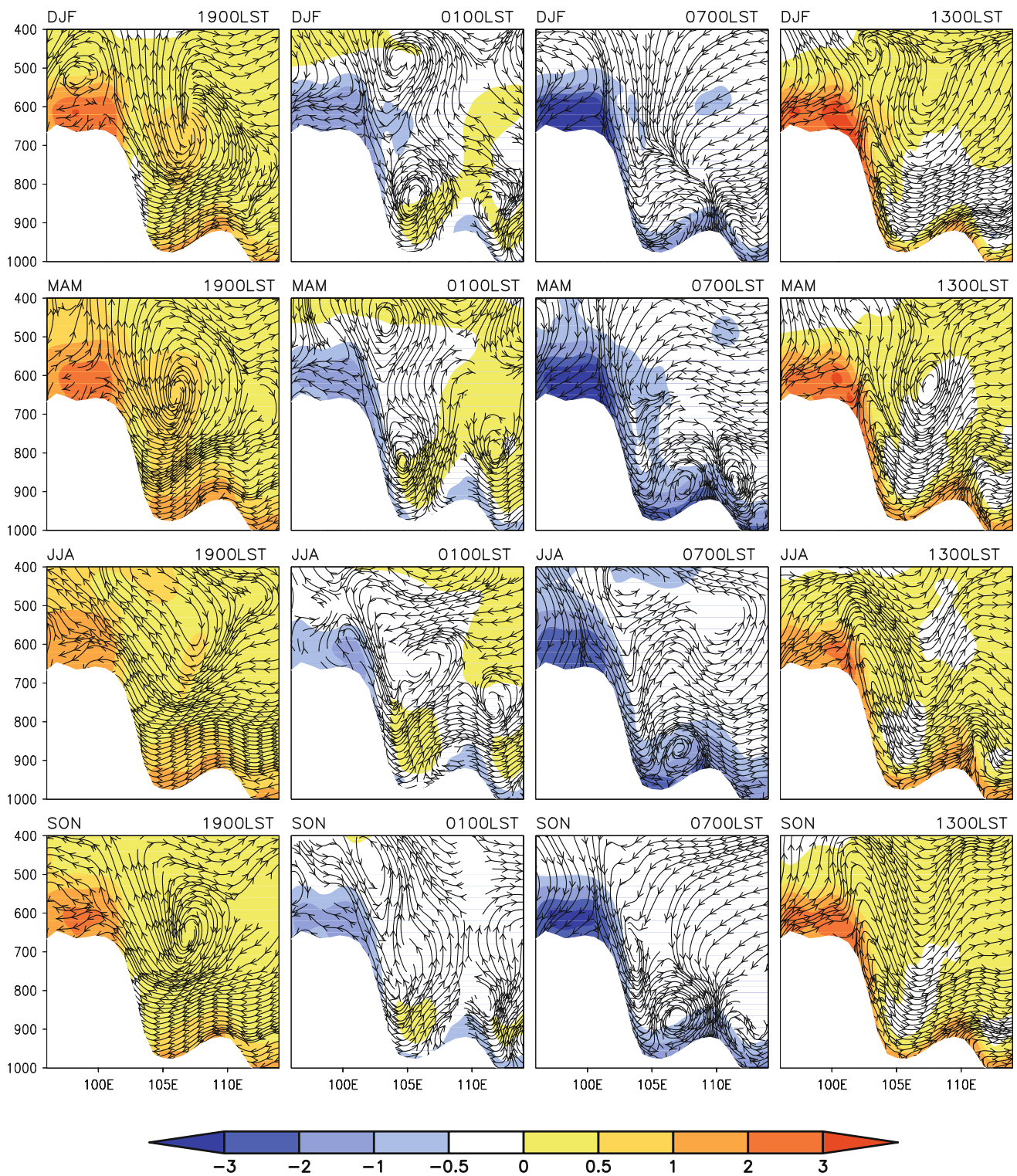
Fig. 14 Profile of diurnal variation of anomalous vertical circulation (zonal wind and 10 times of vertical velocity, *streamline*) and anomalous potential temperature (K, *shaded*) along the latitude of 30°N for (*top row*) DJF, (*second row*) MAM, (*third row*) JJA and (*bottom row*) SON from their daily means. From *left* to *right*, the columns are for 1900LST, 0100LST, 0700LST and 1300LST, respectively. The *vertical axis* denotes pressure level (hPa)
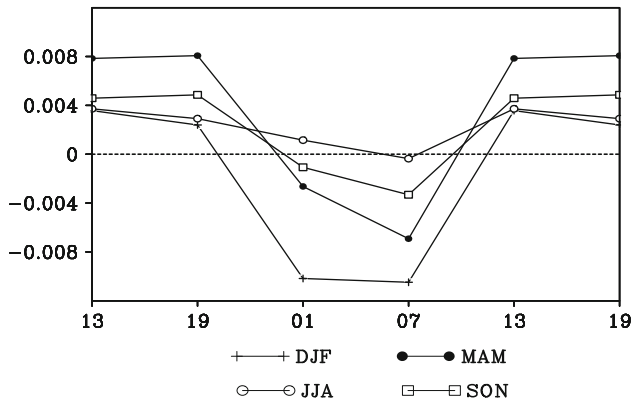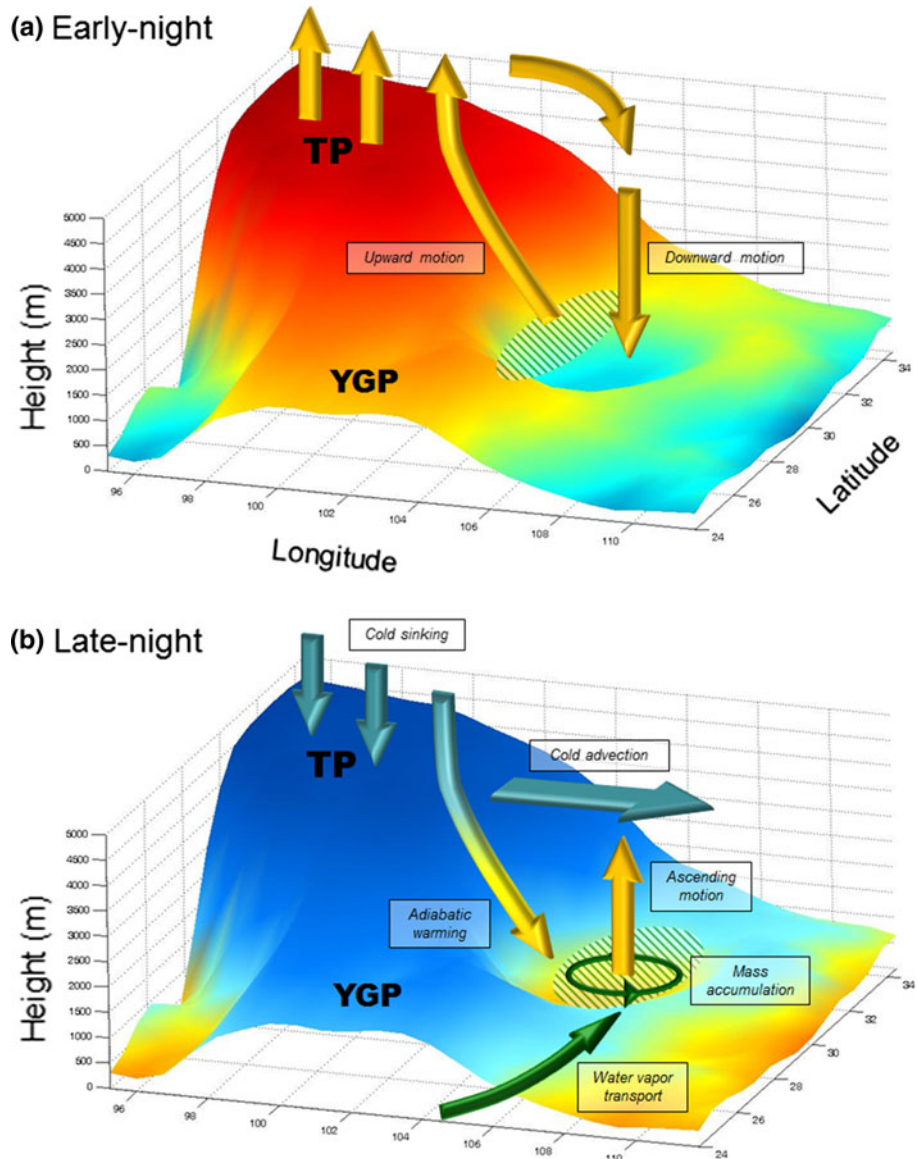
Fig. 15 The diurnal cycle of zonal advection of potential temperature ($-u\frac{\partial\theta}{\partial x}$, unit: 10^{-3} K s^{-1}) at 550 hPa over the position (30°N, 105°E) for the seasons of DJF, MAM, JJA and SON. The horizontal axis signifies the LST

water vapor from lower level in the central and eastern basin, favorable for the occurrence of nocturnal precipitation.

5 Summary and conclusion

Many previous studies focus on the nocturnal precipitation in the Sichuan Basin in summer. This work expands the study on the diurnal cycle of precipitation in the Sichuan Basin to four seasons of the whole year. Results show that nocturnal precipitation has a quasi-stationary feature in the basin during the whole year. It appears not only in summer but also in other three seasons. In particular, the areas with nocturnal maximal precipitation in spring and autumn are more remarkable than that in summer. There is a prominent

Fig. 16 Schematic diagram illustrating the different factors on the nocturnal precipitation at **a** early-night and **b** late-night. The *green diagonal shade* denotes the area where the diurnal phase of precipitation peaks at each time

eastward timing delay of the diurnal precipitation peak between the western basin and the central and eastern basin. That is the maximal precipitation occurs at early-night (1800–0000LST) in the western basin, but appears at late-night (0000–0600LST) in the central and eastern basin. Most of the nocturnal convection along 30°N might be caused by local forcing, and there is rarely propagation of the convection originated from the plateau.

The TP plays an essential role in the formation of this quasi-stationary nocturnal precipitation in the Sichuan Basin. To summarize, a schematic diagram is shown in Fig. 16, the rainfall in western basin is much closely linked to the thermal condition of the plateau plain. At early-night (Fig. 16a), the western basin is dominated by upward motion which is caused by a strong warming at the near surface of the TP. The strong warming over the TP leads to ascendance over the TP and upslope wind along the eastern lee side of the TP, favoring strong precipitation at early-night in the western basin.

The physical mechanism for nocturnal precipitation in the central and eastern basin is different from that in the western basin. There are three coexisting factors contributing to the late-night peak of precipitation in the central and eastern basin (Fig. 16b):

1. There is a strengthening southwesterly air current flowing around the southeastern edge of the YGP at low level of the troposphere at late-night than in other times. It enters the eastern part of the basin and causes a stronger cyclonic rotation in the central basin, favoring ascendance at late-night. This air current from south also brings abundant water vapor into the basin, which is propitious for nocturnal precipitation.
2. After sunset, the atmosphere at near surface of the TP cools down substantially, creating cold downdraft and divergence over the TP. There is an accumulation of warmer air mass in the central basin, which comes from the southeastern edge of the YGP. As the cold air over the TP moves downslope along the eastern lee side of the TP to the central basin, it causes a diabatic warming at low level of the troposphere (from 900 to 800 hPa) in the basin. Then warm air arises in the center and east of the basin, creating atmospheric instability.
3. The cooling and strong divergence over the TP causes an eastward cold advection at middle level of the troposphere in the central basin at late-night. The lower level warm updraft encounters this cold advection in the central and eastern basin, which eases the occurrence of nocturnal precipitation.

Future studies will examine the respective contributions of different mechanisms involved in the nocturnal precipitation in the Sichuan Basin. We are also planning to examine how climate models involved in future climate projection reproduce this phenomenon of nocturnal precipitation in the Sichuan Basin and the associated physical mechanisms.

References

Bao X, Zhang F, Sun J (2011) Diurnal variations of warm-season precipitation east of the Tibetan plateau over China. Mon Wea Rev 139(9):2790–2810

Carbone RE, Tuttle JD (2008) Rainfall occurrence in the U.S. warm season: the diurnal cycle. J Clim 21:4132–4146

Chen G, Sha W, Iwasaki T (2009) Diurnal variation of precipitation over southeastern China: spatial distribution and its seasonality. J Geophys Res 114:D13103. doi:10.1029/2008JD011103

Chen H, Yu R, Li J, Yuan W, Zhou T (2010) Why nocturnal long-duration rainfall presents an eastward-delayed diurnal phase of rainfall down the Yangtze River valley. J Clim 23:905–917

Dai A, Lin X, Hsu K (2007) The frequency, intensity, and diurnal cycle of precipitation in surface and satellite observations over low- and mid-latitudes. Clim Dyn 29:727–744. doi:10.1007/s00382-007-0260-y

Dee DP, Uppala SM, Simmons AJ et al (2011) The ERA-Interim reanalysis: configuration and performance of the data assimilation system. Quart J R Meteorol Soc 137:553–597. doi:10.1002/qj.828

Fujinami H, Nomura S, Yasunari T (2005) Characteristics of diurnal variations in convection and precipitation over the southern Tibetan Plateau during summer. SOLA 1:49–52

He H, Zhang F (2010) Diurnal variations of warm-season precipitation over Northern China. Mon Wea Rev 138:1017–1025. doi:10.1175/2010MWR3356.1

Huang HL, Wang CC, Chen GTJ, Carbone RE (2010) The role of diurnal solenoidal circulation on propagating rainfall episodes near the eastern Tibetan Plateau. Mon Wea Rev 138:2975–2989

Joyce RJ, Janowiak JE, Arkin PA, Xie P (2004) CMORPH: a method that produces global precipitation estimates from passive microwave and infrared data at high spatial and temporal resolution. J Hydromet 5:487–503

Li Y, Yu R, Xu Y et al (2003) The formation and diurnal changes of stratiform clouds in southern China. Acta Meteorol Sin 61:733–743 (in Chinese)

Li J, Yu R, Zhou T (2008) Seasonal variation of the diurnal cycle of rainfall in southern contiguous China. J Clim 21:6036–6043

Lin X, Randall DA, Fowler LD (2000) Diurnal variability of the hydrologic cycle and radiative fluxes: comparisons between observations and a GCM. J Clim 13:4159–4179

Liu C, Moncrieff MW (1998) A numerical study of the diurnal cycle of tropical oceanic convection. J Atmos Sci 55:2329–2344

Lu J (1942) Nocturnal precipitation in Bashan Mountain. Acta Meteor Sin 16:36–53 (in Chinese)

Shen Y, Feng M, Zhang H, Gao F (2010a) Interpolation methods of China daily precipitation data. J Appl Meter Sci 21(3):279–286

Shen Y, Xiong A, Wang Y, Xie P (2010b) Performance of high-resolution satellite precipitation products over China. J Geophys Res 115:D02114. doi:10.1029/2009JD012097

Shen Y, Pan Y, Yu J, Zhao P (2012) Quality Assessment of hourly merged precipitation products over China. Trans Atmos Sci (in press, in Chinese)

Tripoli GJ, Cotton WR (1989) Numerical study of an observed orogenic mesoscale convective system. Part II: analysis of governing dynamics. Mon Wea Rev 117:305–328

Ye D, Gao Y (1979) The meteorology of the Qinghai-Xizang (Tibet) plateau. Science Press, Beijing

Yu R, Zhou T, Xiong A, Zhu Y, Li J (2007a) Diurnal variations of summer precipitation over contiguous China. Geophys Res Lett 34:L01704. doi:10.1029/2006GL028129

Yu R, Xu Y, Zhou T, Li J (2007b) Relation between rainfall duration and diurnal variation in the warm season precipitation over central eastern China. Geophys Res Lett 34:L13703. doi:10.1029/2007GL030315

Yu R, Yuan W, Li J, Fu Y (2009) Diurnal phase of late-night against late-afternoon of stratiform and convective precipitation in summer southern contiguous China. Clim Dyn. doi:10.1007/s00382-009-0568-x

Yu J, Shen Y, Pan Y, Xu B (2011) Bias adjustment of high spatial/temporal resolution satellite precipitation estimation relying on gauge-based precipitation over China. In: Abstracts of Conventions for Meteorological Telecommunication and Information Technology Committee and National Meteorological Information Center, Chinese Meteorological Society. (in Chinese)

Yuan W, Yu R, Zhang M, Lin W, Chen H and Li J (2011) Regimes of diurnal variation of summer rainfall over the subtropical East Asia. J Clim. doi:10.1175/JCLI-D-11-00288.1

Zeng Q, Yu R, Peng G, Chai F (1994) Research on "Ya-An-Tian-Lou". Part III: physical structure and possible mechanism. Chin J Atmos Sci 18:649–659 (in Chinese)

Zhao Z, Leung LR, Qian Y (2005) Characteristics of diurnal variations of precipitation in China for the recent years. CLIVAR exchanges, No. 3, International CLIVAR Project Office, Southampton, UK, pp 24–26

Zhou T, Yu R, Chen H, Dai A, Pan Y (2008) Summer precipitation frequency, intensity, and diurnal cycle over China: a comparison of satellite data with rain gauge observations. J Clim 21:3997–4010